



Adding DSC PWI and DWI to BT-RADS can help identify postoperative recurrence in patients with high-grade gliomas

Yuelong Yang¹ · Yunjun Yang¹ · Xiaoling Wu¹ · Yi Pan² · Dong Zhou³ · Hongdan Zhang² · Yonglu Chen¹ · Jiayun Zhao¹ · Zihua Mo¹ · Biao Huang¹

Received: 12 November 2019 / Accepted: 27 December 2019 / Published online: 4 January 2020
© Springer Science+Business Media, LLC, part of Springer Nature 2020

Abstract

Background The Brain Tumor Reporting and Data System (BT-RADS) category 3 is suitable for identifying cases with intermediate probability of tumor recurrence that do not meet the Response Assessment in Neuro-Oncology (RANO) criteria for progression. The aim of this study was to evaluate the added value of dynamic susceptibility contrast-enhanced perfusion-weighted imaging (DSC PWI) and diffusion-weighted imaging (DWI) to BT-RADS for differentiating tumor recurrence from non-recurrence in postoperative high-grade glioma (HGG) patients with category 3 lesions.

Methods Patients with BT-RADS category 3 lesions were included. The maximal relative cerebral blood volume ($rCBV_{max}$) and the mean apparent diffusion coefficient (ADC_{mean}) values were measured. The added value of DSC PWI and DWI to BT-RADS was evaluated by receiver operating characteristic (ROC) curve analysis.

Results Fifty-one of 91 patients had tumor recurrence, and 40 patients did not. There were significant differences in $rCBV_{max}$ and ADC_{mean} between the tumor recurrence group and non-recurrence group. Compared to BT-RADS alone, the addition of DSC PWI to BT-RADS increased the area under curve (AUC) from 0.76 (95% confidence interval [CI] 0.66–0.84) to 0.90 (95% CI 0.81–0.95) for differentiating tumor recurrence from non-recurrence. The addition of DWI to BT-RADS increased the AUC from 0.76 (95% CI 0.66–0.84) to 0.88 (95% CI 0.80–0.94). The combination of BT-RADS, DSC PWI, and DWI exhibited the best diagnostic performance (AUC = 0.95; 95% CI 0.88–0.98) for differentiating tumor recurrence from non-recurrence.

Conclusion Adding DSC PWI and DWI to BT-RADS can significantly improve the diagnostic performance for differentiating tumor recurrence from non-recurrence in BT-RADS category 3 lesions.

Keywords Structured template · High-grade glioma · Recurrence · Perfusion magnetic resonance imaging · Diffusion magnetic resonance imaging

Introduction

Glioma is the most common tumor of all primary central nervous system tumors, and high-grade gliomas (HGG) account for about 60% of lesions [1]. The recurrence rate and mortality for patients with HGG are still high due to the tumor's invasiveness and rapid growth, regardless of multidisciplinary combination therapy. The standard

treatment protocol is total or subtotal resection, followed by concomitant radio-chemotherapy (CCRT) and adjuvant chemotherapy in order to improve overall survival (OS) [2, 3]. Treatment-related changes, especially pseudoprogression and radiation necrosis, are difficult to distinguish from tumor recurrence on conventional magnetic resonance imaging (MRI) [4].

A series of response evaluation criteria to evaluate the effectiveness of glioma treatment have been proposed, and include the Levin, World Health Organization, MacDonald, and Response Assessment in Neuro-Oncology (RANO) criteria [5]. However, they are not widely incorporated into the radiology reports in routine clinical work because of their complex processes and high inter- and intra-observer variability. The Brain Tumor Reporting and Data System

Yuelong Yang and Yunjun Yang are Co-first authors and also contributed equally to this study.

✉ Biao Huang
huangbiao@gdph.org.cn

Extended author information available on the last page of the article

(BT-RADS) is a simplified classification system for assessing post-treatment brain tumors [6], and is more effective with respect to communication among radiologists and clinicians [7, 8]. In which category 3 is capable of identifying cases with different probability of tumor recurrence overcoming the limitations of the RANO criteria that fails to differentiate tumor recurrence from treatment-related changes. However, the ability of BT-RADS to differentiate category 3 lesions into tumor recurrence versus non-recurrence is often confusing for clinicians and radiologists, because tumor recurrence and non-recurrence may occur in each of the 3 subcategories. So it is indispensable to identify them due to different treatment methods and prognosis.

Dynamic susceptibility contrast-enhanced perfusion-weighted imaging (DSC PWI) and diffusion-weighted imaging (DWI) can reflect angiogenesis and movement of water molecules, respectively [9], and studies have shown they may be valuable for differentiating tumor recurrence from treatment-related changes [10, 11]. We hypothesized that DSC PWI and DWI can add information that is useful for clarifying the characteristics of category 3 lesions. Therefore, the objective of this study was to determine the added value of DSC PWI and DWI for differentiating tumor recurrence from non-recurrence in BT-RADS category 3 lesions in postoperative HGG patients.

Materials and methods

Patients

This retrospective study was approved by the Institutional Review Board of our hospital. Because of the retrospective nature of the study, the requirement of informed patient consent was waived. Brain MRI data obtained at our hospital from January 2015 through December 2018 were reviewed to identify postoperative patients who were diagnosed with BT-RADS category 3 lesions during follow-up. Criteria for inclusion in the analysis were: (1) Diagnosis of histologically confirmed HGG after initial surgery, based on World Health Organization criteria; (2) Treatment with CCRT and adjuvant chemotherapy; (3) Increasing enhancing lesions classified as BT-RADS category 3 in comparison with prior imaging data; (4) Conventional MR imaging, DSC PWI, and DWI were performed within 72 h after surgical removal of the tumor; (5) Repeat resection or follow-up information containing the aforementioned imaging studies performed every 3 to 6 months, to determine tumor recurrence after treatment. Patients with incomplete follow-up data, and those whose MR images were of inferior quality that prevented the analyses required for this study were excluded. The BT-RADS category of all cases was independently assessed online (<https://btrads.com/publications/>) in the light

of conventional MR imaging data by a neuroradiologist with more than 10 years of experience.

MR image acquisition

MR images were obtained using a 3.0 T Philips Ingenia scanner, with an 8-channel head coil. Apart from conventional T1-weighted imaging (T1WI), T2WI, T2-FLAIR, and contrast-enhanced T1WI held, functional perfusion and diffusion MR images were also obtained. The parameters for obtaining perfusion-weighted gradient-echo echo-planar images were: TR = 17 ms, TE = 8 ms, FOV = 230 mm, matrix size = 128 × 128, flip angle = 7°, slice thickness = 5 mm, intersection gap = 0 mm. The parameters for obtaining single-shot echo-planar images were: TR = 2662 ms, TE = 90 ms, FOV = 230 mm, matrix size = 256 × 256, flip angle = 90°, slice thickness = 5 mm, intersection gap = 1 mm, b-values = 0 and 1000 s/mm².

Multi-section perfusion-weighted image data were obtained every second for a total of 1 min and 30 s, with administration of the gadopentetate dimeglumine (Magnevist; Bayer HealthCare Pharmaceuticals, Wayne, New Jersey) injection beginning after 10 s. DSC PWI was performed during the administration with an intravenous bolus injection of gadopentetate dimeglumine, along with a standard dose (0.2 ml/kg of body weight, maximum dose of 20 ml), at a rate of 2.5 ml/s. The bolus of gadopentetate dimeglumine was followed by a 20 ml saline flush at exactly the same rate, with an MRI-compatible power injector.

Image analysis

Original DSC PWI data were transferred to a radiology workstation (Advantage Workstation, Philips, Amsterdam, Holland), and the transverse T2*-weighted pulse sequence data were visualized with the Perfusion Software Package. Parametric perfusion maps were obtained on a voxel-by-voxel basis, and cerebral blood volume (CBV) was calculated based on signal intensity–time curves that were developed from changes in relaxivity. Three small (15–20 pixels) circular regions of interest (ROIs) were placed in the enhancing lesion where the highest CBV was noted, and the maximal CBV of the 3 ROIs was used as the CBV_{max}. The internal reference CBV was obtained from an ROI of the same pixel size placed in the contralateral normal white matter. The relative CBV_{max} (rCBV_{max}) ratio was defined as the CBV_{max} divided by the internal reference CBV. The rCBV_{max} was used in the quantitative data analysis.

The DWI data were transferred to radiology workstation (Advantage Workstation), and were reprocessed to develop apparent diffusion coefficient (ADC) maps at b = 1000 s/mm² using post-processing software. The ROI was drawn selectively in a section of the DWI matching the largest

transverse lesion level on contrast T1-weighted images three times, and then they were copied to the ADC map. Because DWI was at the same level of the ADC maps, the ROI setting between the 2 sets of data were uniform. The average of the 3 ROIs on the ADC maps was defined as the mean ADC (ADC_{mean}). Areas of necrosis, cysts, hemorrhage, or blood vessels in the contrast T1-weighted images were not included in any of the ROIs.

BT-RADS category

BT-RADS score category was proposed by a team of experienced clinicians and neuroradiologists to standard report blinded to the DSC PWI and DWI data. Enlarged enhancing lesions were classified on the 0–4 scoring system [6], based on conventional imaging features and clinical symptoms considered in light of the previous imaging data. Baseline lesions and imaging data were defined as BT-RADS Category 0. Lesions with improvements from previous imaging data were defined as BT-RADS Category 1. Lesions whose imaging features were similar to those of the previous imaging were defined as BT-RADS Category 2. Lesions with imaging data that suggested growth or progression were defined as BT-RADS Category 3 or 4, as appropriate. Category 3 lesions were divided into 3 subtypes: Category 3a were likely to represent treatment-related changes; Category 3b represented an indeterminate mix of treatment-related changes and tumor progression; Category 3c represented tumor progression. Lesion BT-RADS classification taking into account enhancing components, FLAIR components, and mass effect was determined as described in a previously published study [6].

Diagnostic criteria for recurrence

The diagnosis of tumor recurrence was made based on pathological examination of a tissue specimen obtained from repeat surgery or stereotactic biopsy, or clinical and radiological follow-up observations. Non-recurrence of the tumor was defined as the complete absence of tumor cells or scarce tumor cells (<25%) on the pathological examination of a tissue specimen [12], as well as improvement or stability of lesion enhancement on follow-up MRI for more than 6 months [2, 13]. Tumor recurrence was defined as >75% tumor cells identified in a tissue specimen [12], or progressively increasing enhancement on follow-up imaging studies.

Statistical analysis

Continuous variables with a normal distribution based on the Durbin-Watson test were presented as mean \pm standard deviation, and compared with the t-test. The Mann–Whitney U-test was used to examine data with a skewed distribution,

and data were expressed as median and interquartile (IQR) range. Categorical variables were presented as frequency (percentage), and were compared with the χ^2 test. Receiver operating characteristic (ROC) curve analysis was performed to determine the diagnostic performance of different parameters, or their combinations, for discriminating tumor recurrence from non-recurrence. Comparisons of the areas under the ROC curve (AUC) for different combinations were interpreted by the Z test. The accuracy, sensitivity, specificity, positive predictive value (PPV), and negative predictive value (NPV) based on optimum cutoffs were compared. All statistical analyses were performed with SPSS version 22.0 statistical software for Windows (SPSS, Chicago, Illinois, USA), and MedCalc version 17.5.3 (Mariakerke, Belgium). A statistical difference was considered significant when the p value was <0.05.

Results

Patient baseline characteristics

A total of 91 patients who met the inclusion criteria were identified in the medical records. There were 53 males and 38 females, with a mean age of 48.7 ± 14.2 years (range 9 to 77 years). Of the 91 patients, 51 had tumor recurrences, and 40 did not have a recurrence. Twenty-three (45.1%) of the 51 tumor recurrences and 11 (27.5%) of 40 non-recurrences were confirmed by a second surgery or stereotactic biopsy, and 28 (54.9%) of the 51 tumor recurrences and 29 (72.5%) of 40 non-recurrences were confirmed by standard clinical follow-up. Patient demographic and clinical data by recurrence group are summarized in Table 1. Karnofsky Performance Status (KPS) Scale score and the primary surgery method were significantly different between the tumor recurrence and non-recurrence groups ($p = 0.039$ and 0.034 , respectively). The time interval from CCRT to identification of an abnormal enlarging enhanced lesion was significantly shorter in the non-recurrence group than the recurrence group (6.6 ± 3.4 months vs. 10.5 ± 5.0 months, $p < 0.001$). Other demographic and clinical data, such as age, sex, tumor grade, isocitrate dehydrogenase (IDH) genotype, and enhancing lesion diameter were not different between the two groups (all, $p > 0.05$).

Diagnostic performance of the single imaging method

Using the BT-RADS classification, 28 patients were Category 3a, 26 Category 3b, and 37 Category 3c. The incidence of recurrence for each BT-RADS category is shown in Table 2. The recurrence rate for BT-RADS Category 3a was 21.4% (6/28), for Category 3b was 61.5% (16/26), and

Table 1 Clinical and demographic data in the recurrence and non-recurrence groups

Variables	Total (n=91)	Recurrence (n=51)	Non-recurrence (n=40)	<i>p</i> value
Age (years)	48.7 ± 14.2	47.8 ± 14.5	50.0 ± 13.8	0.454
Sex				0.066
Male	53 (58.2)	34 (66.7)	19 (47.5)	
Female	38 (41.8)	17 (33.3)	21 (52.5)	
Enhancing lesion diameter (cm)				0.662
≥ 5	44 (48.4)	23 (45.1)	21 (52.5)	
< 5	47 (51.6)	28 (54.9)	19 (47.5)	
KPS score				0.039*
≥ 70	60 (66.0)	29 (56.9)	31 (77.5)	
< 70	31 (34.0)	22 (43.1)	9 (22.5)	
Primary surgery				0.034*
Gross total resection	70 (76.9)	35 (68.6)	35 (87.5)	
Partial resection	21 (23.1)	16 (31.4)	5 (12.5)	
Grade				0.428
III	29 (31.9)	18 (35.3)	11 (27.5)	
IV	62 (68.1)	33 (64.7)	29 (72.5)	
IDH genotype				0.410
Mutation	22 (24.2)	14 (27.5)	8 (20.0)	
Wild	69 (75.8)	37 (72.5)	32 (80.0)	
Time interval (months)	8.8 ± 4.8	10.5 ± 5.0	6.6 ± 3.4	< 0.001*

Data presented as mean ± SD or n (%)

KPS Karnofsky performance status, *IDH* isocitrate dehydrogenase

*Statistically significant

Table 2 Comparisons of the single imaging method between the tumor recurrence and non-recurrence groups

Variables	Recurrence (n=51)	Non-recurrence (n=40)	<i>P</i> value	Cutoff	AUC
BT-RADS			< 0.001		0.76
3a	6 (11.8)	22 (55.0)			
3b	16 (31.4)	10 (25.0)			
3c	29 (56.8)	8 (20.0)			
<i>rCBV</i> _{max}	2.3 (1.9–2.7)	1.3 (1.1–1.6)	< 0.001	1.6	0.87
<i>ADC</i> _{mean} (× 10 ⁻³ mm ² /s)	0.8 (0.7–1.0)	1.3 (1.2–1.4)	< 0.001	1.0	0.85

Data presented as median (IQR) or n (%)

BT-RADS Brain Tumor Reporting and Data System, *rCBV*_{max} maximum relative cerebral blood volume, *ADC*_{mean} mean apparent diffusion coefficient, *AUC* area under the ROC curve

for Category 3c was 78.4% (29/37). The BT-RADS categories differed significantly between the two groups, and analysis indicated that the BT-RADS scoring system had an *AUC* = 0.76 for discriminating tumor recurrence versus non-recurrence. The analysis of single quantitative functional imaging parameters indicated that *rCBV*_{max} and *ADC*_{mean} were significantly different between the two groups. The *rCBV*_{max} of the tumor recurrence group (2.3, IQR: 1.9–2.7) was significantly higher than that of the non-recurrence tumor group (1.3, IQR: 1.1–1.6) (*p* < 0.001). The *ADC*_{mean} of the tumor recurrence group (0.8, IQR: 0.7–1.0 × 10⁻³ mm²/s)

was significantly lower than that of the non-recurrence group (1.3, IQR: 1.2–1.4 × 10⁻³ mm²/s) (*p* < 0.001). ROC analysis indicated that *rCBV*_{max} and *ADC*_{mean} exhibited similar *AUC*s for discriminating between tumor recurrence and non-recurrence (0.87 vs. 0.85, respectively, *Z* = 0.26, *p* = 0.79).

Added value of DSC PWI and DWI to BT-RADS

The ROC curve analyses for different combinations of data for distinguishing tumor recurrence from non-recurrence are shown in Fig. 1. The *AUC* of the combination

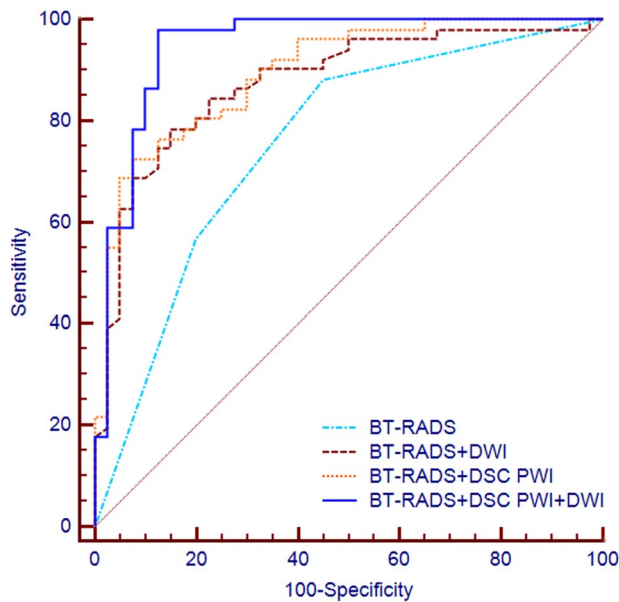


Fig. 1 Comparison of ROC curve analyses for different combinations. The combination of BT-RADS + DSC PWI + DWI presents the highest diagnostic value, and the AUC was 0.95 (95% CI 0.88–0.98) with a significance level of $p < 0.05$ to any in the other three combinations

of BT-RADS + DSC PWI was similar to that of the combination of BT-RADS + DWI (0.90 vs. 0.88, respectively, $Z = 0.52$, $p = 0.61$). The AUCs of both combinations were significantly larger than that of BT-RADS alone (0.90 vs. 0.76, $Z = 3.35$, $p < 0.01$; 0.88 vs. 0.76, $Z = 2.73$, $p < 0.01$, respectively). The diagnostic performance of BT-RADS was significantly improved when it was combined with $rCBV_{max}$ (DSC PWI) and ADC_{mean} (DWI) (AUC = 0.95; 95% CI 0.88–0.98), and their combination of BT-RADS + DSC PWI + DWI manifested the best diagnostic performance for distinguishing tumor recurrence from non-recurrence ($p < 0.05$ for any comparison with the other combinations). The cutoff values of $rCBV_{max}$ and ADC_{mean} utilized to the differentiation of tumor recurrence and non-recurrence were 1.6, $1.0 \times 10^{-3} \text{ mm}^2/\text{s}$, respectively (Table 2). Typical cases of tumor recurrence and non-recurrence are shown in Fig. 2 and Fig. 3, respectively. The AUC, accuracy, sensitivity, specificity, PPV, and NPV of each combination of MR data are summarized in Table 3, in which the combination of BT-RADS + DSC PWI + DWI exhibited the highest accuracy (0.92), sensitivity (0.98; 95% CI 0.88–0.99), and NPV (0.97; 95% CI 0.83–0.99).

Discussion

We have benefited greatly from the implementation of BT-RADS at our institution for the postoperative surveillance for glioma on account of its characteristics of consistency

and conciseness. However, the heterogeneity and variability of BT-RADS Category 3 lesions in patients with HGG did not allow differentiation of tumor recurrence from treatment-related changes on conventional MRI. We found that adding additional parameters such as $rCBV_{max}$ and ADC_{mean} to BT-RADS can significantly improve diagnostic performance for differentiating tumor recurrence from non-recurrence. Accurate identification of tumor recurrence in BT-RADS Category 3 lesions is important because patients with recurrence may be candidates for additional treatment, while those without a recurrence may not need further treatments.

The addition of DSC PWI and DWI to BT-RADS demonstrated the optimal value for characterizing Category 3 lesions. Identification of tumor recurrence is important for selecting treatment, and in this study the combination of DSC PWI, DWI, and BT-RADS resulted in the best diagnostic performance for distinguishing tumor recurrence from non-recurrence, and the combination had the highest AUC and accuracy, and best sensitivity and NPV. We believe this finding is likely because functional imaging provide more comprehensive information with respect to microvascular density and lesion pathophysiology [14, 15]. Consequently, based on these results we recommend that patients with suspicious BT-RADS Category 3 enhancing lesions should receive DSC PWI and DWI imaging examinations.

Standardized follow-up care for post-treatment patients is very important for monitoring outcomes. Although several response evaluation criteria have been developed to assess clinical and imaging responses in the treatment of HGG [5], they are more widely used in clinical trials, rather than routine clinical practice. In addition, newer immunotherapies for HGG may lead to complex inflammatory responses, which are beyond the scope of these criteria [16, 17]. BT-RADS attempts to evade using the terms pseudoprogression, pseudoresponse, or radiation necrosis. In fact, although pseudoprogression and radiation necrosis are different clinical entities, these terms have been occasionally interchanged [5]. Although simplistic, BT-RADS is useful for guiding treatment and increases the participation of radiologists in patient management [8].

Differentiation of tumor recurrence from non-recurrence in BT-RADS Category 3 lesions is essential for avoiding unnecessary repeat surgery, hasty discontinuation of adjuvant TMZ or its substitution for effective second-line or salvage therapies. The microvascular sensitivity of DSC PWI can reflect the degree of microangiogenesis and blood supply [18]. The $rCBV_{max}$, the most commonly used semiquantitative parameter, demonstrates relatively good accuracy for distinguishing tumor progression from treatment-related changes [19]. DSC PWI has been proven to be useful for evaluating the proliferative activity and pathology of post-treatment HGG. Prior studies have indicated that a lower $rCBV_{max}$ is associated with treatment-related changes, such

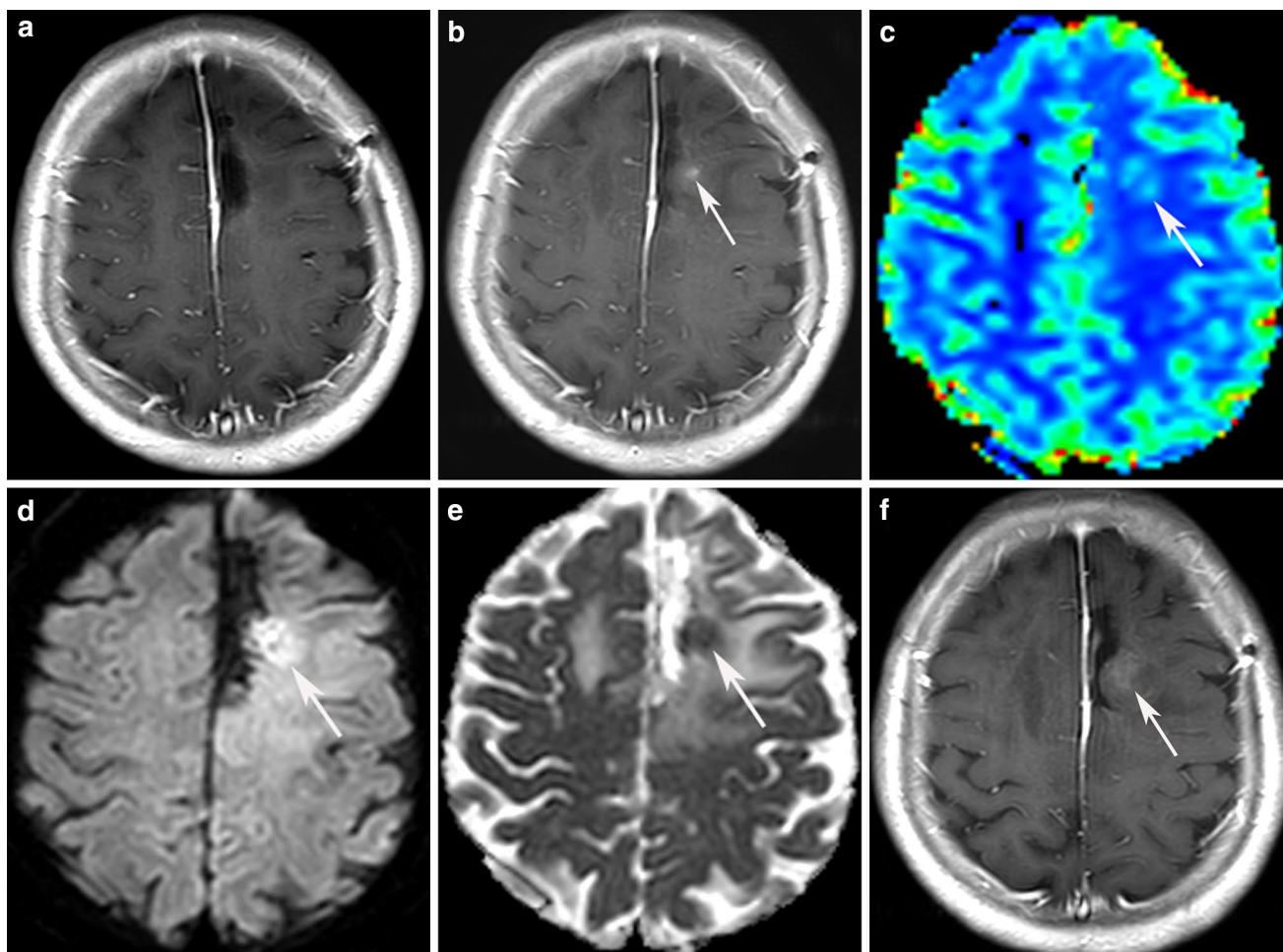


Fig. 2 A 54-year-old female with IDH wildtype anaplastic astrocytoma. **a** No abnormal enhancement was found 10 months after completing radiotherapy on Gd-enhanced T1 weighted image (Gd-T1WI). **b** Gd-T1WI showed asymmetric new enhanced lesion defined as Category 3b (arrow) in the left frontal lobe 16 months after completing radiotherapy. **c** DSC PWI showed hyperperfusion (arrow) in the left

frontal lobe. **d,e** Restricted diffusion was observed in the enhanced lesion on DWI and ADC map (arrow). **f** The enhancement further enlarged with an increased mass effect 19 months after completing radiotherapy on Gd-T1WI. Consequently, the enhanced lesion in the left frontal lobe was deemed a tumor recurrence

as early pseudoprogression apart from late radiation necrosis rather than tumor progression [20, 21]. Interestingly, pseudoprogression is associated with a favorable prognosis and improved survival [10, 22]. On the contrary, late radiation necrosis is associated with severe morbidity that often requires further treatment. As a functional MRI method, DSC PWI can improve the diagnostic efficiency of conventional MRI. Our results indicated that when DSC PWI data is added to BT-RADS, the AUC, accuracy, specificity, and PPV increase, although the increase in specificity (90% vs. 55%) was accompanied by a slight decrease in sensitivity (73% vs. 88%).

DWI reflects the viability and structure of lesions on a cellular level. Quantitative analysis has shown that the ADC_{mean} value in recurrent tumors is lower, a finding indicative of reduced water movement [23]. Chu et al. [24]

reported increases in ADC values with treatment-related changes at both standard- and high-b-value DWI. Our results are consistent with those of Cha et al. [25], who reported significantly lower ADC values in postoperative glioma patients with tumor recurrence as compare to those with treatment-related changes. These findings are possibly because solid components of tumors with reduced extracellular space are more likely to lead to lower ADC values than cystic contents or a solid–liquid mixture that can result from treatments. In current study, we showed that DWI can increase the diagnostic performance of BT-RADS, with better accuracy, increased specificity, and improved PPV.

A few limitations have been met to the current study. First, the diagnosis was not confirmed by histopathological examination of tissue in all cases. Although pathological confirmation is the most accurate and ideal method, it is not

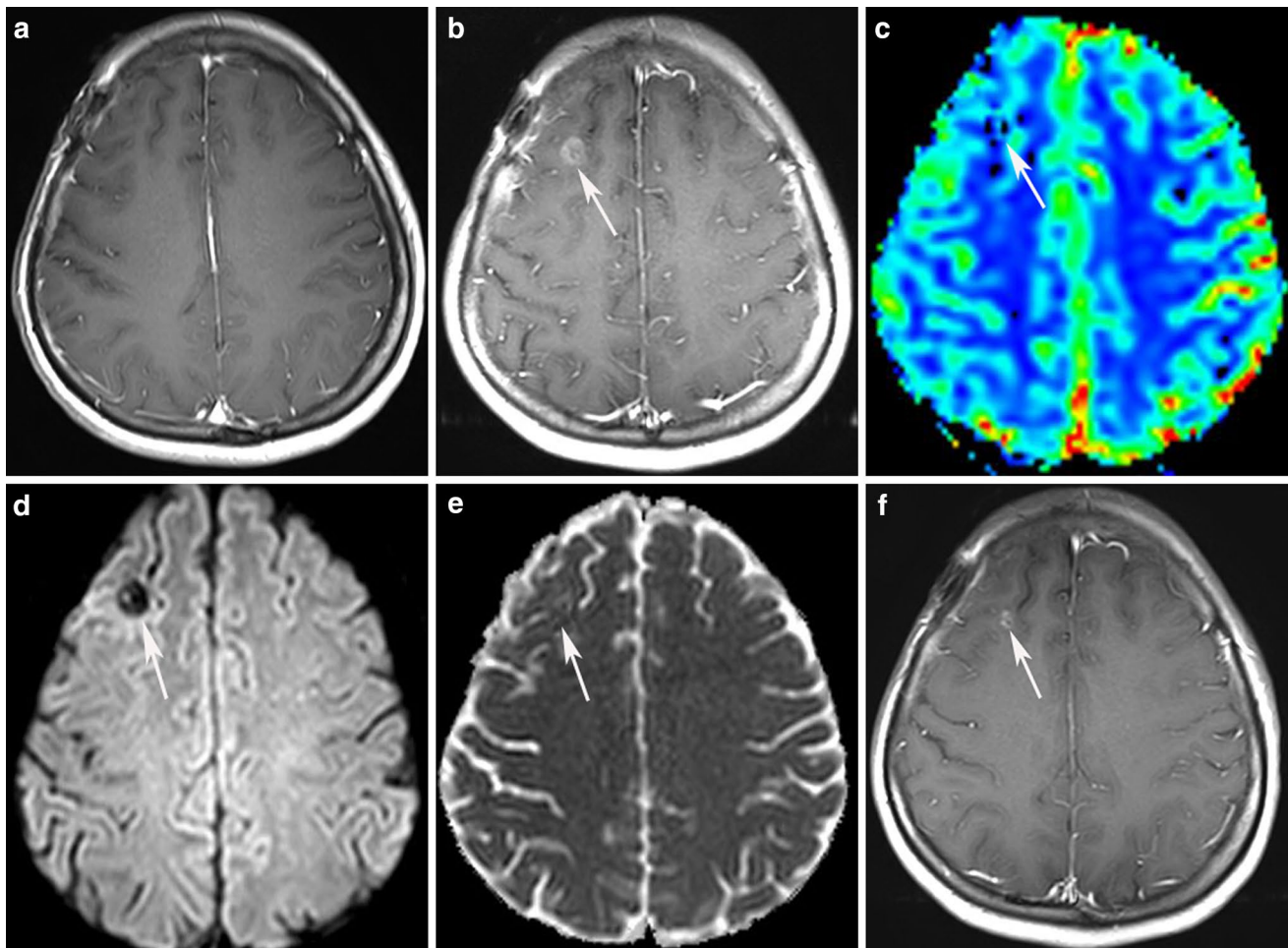


Fig. 3 A 37-year-old female with anaplastic oligodendroglioma with IDH mutation and 1p/19q co-deletion. **a** No abnormal enhancement was found 24 months after completing radiotherapy on Gd-enhanced T1 weighted image (Gd-T1WI). **b** Gd-T1WI showed asymmetric new enhanced lesion defined as Category 3b (arrow) in the right frontal lobe 27 months after completing radiotherapy. **c** DSC PWI showed

asymmetric hypoperfusion (arrow) in the right frontal lobe. **d,e** No restricted diffusion was observed in the enhanced lesion on DWI and ADC map (arrow). **f** The enhancement shrank significantly (arrow) 30 months after completing radiotherapy on Gd-T1WI. Consequently, the enhanced lesion in the right frontal lobe was deemed a radiation-related late injury (tumor non-recurrence)

Table 3 The predictive value of each combination for tumor recurrence

Combinations	AUC (95%CI)	Accuracy	Sensitivity (95%CI)	Specificity (95%CI)	PPV (95%CI)	NPV (95%CI)
BT-RADS	0.76 (0.66–0.84)	0.74	0.88 (0.75–0.95)	0.55 (0.39–0.70)	0.71 (0.59–0.82)	0.79 (0.59–0.91)
BT-RADS + DSC	0.90 (0.81–0.95)	0.80	0.73 (0.58–0.84)	0.90 (0.75–0.97)	0.90 (0.76–0.97)	0.72 (0.57–0.83)
BT-RADS + DWI	0.88 (0.80–0.94)	0.80	0.78 (0.64–0.88)	0.83 (0.67–0.92)	0.85 (0.71–0.93)	0.75 (0.59–0.86)
BT-RADS + DSC + DWI	0.95 (0.88–0.98)	0.92	0.98 (0.88–0.99)	0.85 (0.70–0.94)	0.89 (0.77–0.96)	0.97 (0.83–0.99)

BT-RADS Brain Tumor Reporting and Data System, DSC dynamic susceptibility contrast, DWI diffusion-weighted imaging, AUC area under the ROC curve, CI confidence interval, PPV positive predictive value, NPV negative predictive value

always practical clinically. More than half of the patients (62.6%) were diagnosed based on follow-up clinical and radiological data as an alternative pointer of pathology. Second, $rCBV_{max}$ and ADC_{mean} were measured using a 2D mode

for the maximum anomaly level. Although this technique cannot fully reflect the pathophysiological status of a tumor, it is widely accepted for clinical use and has the advantages of good reproducibility, convenience, and rapidness.

Conclusion

The results of this study indicate that adding DSC PWI and DWI to the conventional MRI can help to identify tumor recurrence in BT-RADS Category 3 lesions. Identification of recurrence may aid in optimizing individual postoperative management of these patients.

Acknowledgements This work was supported by the Key R&D Program of Guangdong Province (Grant No. 2018B030339001); National Natural Science Foundation of China (Grant No. 81671275) and the Fundamental Research Funds for the Central Universities (Grant No. 2018MS27).

Compliance with ethical standards

Conflict of interest The authors declare that the research was conducted in the absence of any commercial or financial relationships that could be construed as a potential conflict of interest.


References

- Ostrom QT, Gittleman H, Truitt G, Boscia A, Kruchko C, Barnholtz-Sloan JS (2018) CBTRUS statistical report: primary brain and other central nervous system tumors diagnosed in the united states in 2011–2015. *Neuro Oncol* 20:iv1–iv86. <https://doi.org/10.1093/neuonc/noy131>
- Ma B, Blakeley JO, Hong X, Zhang H, Jiang S, Blair L, Zhang Y, Heo HY, Zhang M, van Zijl PC, Zhou J (2016) Applying amide proton transfer-weighted MRI to distinguish pseudoprogression from true progression in malignant gliomas. *J Magn Reson Imaging* 44:456–462. <https://doi.org/10.1002/jmri.25159>
- Chinot OL, Wick W, Mason W, Henriksson R, Saran F, Nishikawa R, Carpentier AF, Hoang-Xuan K, Kavan P, Cerna D, Brandes AA, Hilton M, Abrey L, Cloughesy T (2014) Bevacizumab plus radiotherapy-temozolomide for newly diagnosed glioblastoma. *N Engl J Med* 370:709–722. <https://doi.org/10.1056/NEJMoa1308345>
- Galldiks N, Kocher M, Langen KJ (2017) Pseudoprogression after glioma therapy: an update. *Expert Rev Neurother* 17:1109–1115. <https://doi.org/10.1080/14737175.2017.1375405>
- Delgado-Lopez PD, Rinones-Mena E, Corrales-Garcia EM (2018) Treatment-related changes in glioblastoma: a review on the controversies in response assessment criteria and the concepts of true progression, pseudoprogression, pseudoresponse and radionecrosis. *Clin Transl Oncol* 20:939–953. <https://doi.org/10.1007/s12094-017-1816-x>
- Weinberg BD, Gore A, Shu HG, Olson JJ, Duszak R, Voloschin AD, Hoch MJ (2018) Management-based structured reporting of posttreatment glioma response with the brain tumor reporting and data system. *J Am Coll Radiol* 15:767–771. <https://doi.org/10.1016/j.jacr.2018.01.022>
- Gore A, Hoch MJ, Shu HG, Olson JJ, Voloschin AD, Weinberg BD (2019) Institutional implementation of a structured reporting system: our experience with the brain tumor reporting and data system. *Acad Radiol* 26:974–980. <https://doi.org/10.1016/j.acra.2018.12.023>
- Zhang JY, Weinberg BD, Hu R, Saindane A, Mullins M, Allen J, Hoch MJ (2019) Quantitative improvement in brain tumor MRI through structured reporting (BT-RADS). *Acad Radiol* 27:1–5. <https://doi.org/10.1016/j.acra.2019.07.028>
- Forster A, Brehmer S, Seiz-Rosenhagen M, Mildenerger I, Giordano FA, Wenz H, Reuss D, Hanggi D, Groden C (2019) Heterogeneity of glioblastoma with gliomatosis cerebri growth pattern on diffusion and perfusion MRI. *J Neurooncol* 142:103–109. <https://doi.org/10.1007/s11060-018-03068-w>
- Prager AJ, Martinez N, Beal K, Omuro A, Zhang Z, Young RJ (2015) Diffusion and perfusion MRI to differentiate treatment-related changes including pseudoprogression from recurrent tumors in high-grade gliomas with histopathologic evidence. *Am J Neuroradiol* 36:877–885. <https://doi.org/10.3174/ajnr.A4218>
- White ML, Zhang Y, Yu F, Shonka N, Aizenberg MR, Adapa P, Kazmi SAJ (2019) Post-operative perfusion and diffusion MR imaging and tumor progression in high-grade gliomas. *PLoS ONE* 14:1–12. <https://doi.org/10.1371/journal.pone.0213905>
- Wang S, Martinez-Lage M, Sakai Y, Chawla S, Kim SG, Alonso-Basanta M, Lustig RA, Brem S, Mohan S, Wolf RL, Desai A, Poptani H (2016) Differentiating tumor progression from pseudoprogression in patients with glioblastomas using diffusion tensor imaging and dynamic susceptibility contrast MRI. *Am J Neuroradiol* 37:28–36. <https://doi.org/10.3174/ajnr.A4474>
- Tran DK, Jensen RL (2013) Treatment-related brain tumor imaging changes: So-called "pseudoprogression" vs. tumor progression: review and future research opportunities. *Surg Neurol Int* 4:S129–135. <https://doi.org/10.4103/2152-7806.110661>
- Zikou A, Sioka C, Alexiou GA, Fotopoulos A, Voulgaris S, Argyropoulou MI (2018) Radiation necrosis, pseudoprogression, pseudoresponse, and tumor recurrence: imaging challenges for the evaluation of treated gliomas. *Contrast Media Mol Imaging* 2018:1–6. <https://doi.org/10.1155/2018/6828396>
- Kong Z, Yan C, Zhu R, Wang J, Wang Y, Wang R, Feng F, Ma W (2018) Imaging biomarkers guided anti-angiogenic therapy for malignant gliomas. *Neuroimage Clin* 20:51–60. <https://doi.org/10.1016/j.nicl.2018.07.001>
- Rudie JD, Rauschecker AM, Bryan RN, Davatzikos C, Mohan S (2019) Emerging applications of artificial intelligence in neuro-oncology. *Radiology* 290:607–618. <https://doi.org/10.1148/radio.1.2018181928>
- Roth P, Valavanis A, Weller M (2017) Long-term control and partial remission after initial pseudoprogression of glioblastoma by anti-PD-1 treatment with nivolumab. *Neuro Oncol* 19:454–456. <https://doi.org/10.1093/neuonc/now265>
- Seow P, Wong JHD, Ahmad-Annur A, Mahajan A, Abdullah NA, Ramli N (2018) Quantitative magnetic resonance imaging and radiogenomic biomarkers for glioma characterisation: a systematic review. *Br J Radiol* 91:1–22. <https://doi.org/10.1259/bjr.20170930>
- Patel P, Baradaran H, Delgado D, Askin G, Christos P, John Tsiouris A, Gupta A (2017) MR perfusion-weighted imaging in the evaluation of high-grade gliomas after treatment: a systematic review and meta-analysis. *Neuro Oncol* 19:118–127. <https://doi.org/10.1093/neuonc/now148>
- Young RJ, Gupta A, Shah AD, Graber JJ, Chan TA, Zhang Z, Shi W, Beal K, Omuro AM (2013) MRI perfusion in determining pseudoprogression in patients with glioblastoma. *Clin Imaging* 37:41–49. <https://doi.org/10.1016/j.clinimag.2012.02.016>
- Morabito R, Alafaci C, Pergolizzi S, Pontoriero A, Iati G, Bonanno L, Gaeta M, Salpietro FM, Mormina E, Longo M, Granata F (2019) DCE and DSC perfusion MRI diagnostic accuracy in the follow-up of primary and metastatic intra-axial brain tumors treated by radiosurgery with cyberknife. *Radiat Oncol* 14:1–9. <https://doi.org/10.1186/s13014-019-1271-7>
- Kong DS, Kim ST, Kim EH, Lim DH, Kim WS, Suh YL, Lee JI, Park K, Kim JH, Nam DH (2011) Diagnostic dilemma of pseudoprogression in the treatment of newly diagnosed glioblastomas: the role of assessing relative cerebral blood flow volume

- and oxygen-6-methylguanine-DNA methyltransferase promoter methylation status. *Am J Neuroradiol* 32:382–387. <https://doi.org/10.3174/ajnr.A2286>
23. Lee WJ, Choi SH, Park CK, Yi KS, Kim TM, Lee SH, Kim JH, Sohn CH, Park SH, Kim IH (2012) Diffusion-weighted MR imaging for the differentiation of true progression from pseudoprogression following concomitant radiotherapy with temozolomide in patients with newly diagnosed high-grade gliomas. *Acad Radiol* 19:1353–1361. <https://doi.org/10.1016/j.acra.2012.06.011>
 24. Chu HH, Choi SH, Ryoo I, Kim SC, Yeom JA, Shin H, Jung SC, Lee AL, Yoon TJ, Kim TM, Lee SH, Park CK, Kim JH, Sohn CH, Park SH, Kim IH (2013) Differentiation of true progression from pseudoprogression in glioblastoma treated with radiation therapy and concomitant temozolomide: comparison study of standard and high-b-value diffusion-weighted imaging. *Radiology* 269:831–840. <https://doi.org/10.1148/radiol.13122024>
 25. Cha J, Kim ST, Kim HJ, Kim HJ, Kim BJ, Jeon P, Kim KH, Byun HS (2013) Analysis of the layering pattern of the apparent diffusion coefficient (ADC) for differentiation of radiation necrosis from tumour progression. *Eur Radiol* 23:879–886. <https://doi.org/10.1007/s00330-012-2638-4>

Publisher's Note Springer Nature remains neutral with regard to jurisdictional claims in published maps and institutional affiliations.

Affiliations

Yuelong Yang¹ · Yunjun Yang¹ · Xiaoling Wu¹ · Yi Pan² · Dong Zhou³ · Hongdan Zhang² · Yonglu Chen¹ · Jiayun Zhao¹ · Zihua Mo¹ · Biao Huang¹ 

Yuelong Yang
1466537468@qq.com

Yunjun Yang
2012231568@qq.com

Xiaoling Wu
1411889645@qq.com

Yi Pan
panyiff01@163.com

Dong Zhou
zhoudong5413@163.com

Hongdan Zhang
zhhd333@126.com

Yonglu Chen
cyl1791@126.com

Jiayun Zhao
1471430123@qq.com

Zihua Mo
577900893@qq.com

¹ Department of Radiology, Guangdong Provincial People's Hospital, Guangdong Academy of Medical Sciences, 106 Zhongshan 2nd Road, Guangzhou 510080, China

² Department of Radiotherapy, Cancer Center, Guangdong Provincial People's Hospital, Guangdong Academy of Medical Sciences, Guangzhou 510080, China

³ Department of Neurosurgery, Guangdong Provincial People's Hospital, Guangdong Academy of Medical Sciences, Guangzhou 510080, China